AMERICAN SOCIETY FOR MICROBIOLOGY | Molecular and Cellular Biology

Genome-Wide Studies Reveal that H3K4me3 Modification in Bivalent Genes Is Dynamically Regulated during the Pluripotent Cell Cycle and Stabilized upon Differentiation

Rodrigo A. Grandy,[a] Troy W. Whitfield,[b] Hai Wu,[a] Mark P. Fitzgerald,[a] Jennifer J. VanOudenhove,[a] Sayyed K. Zaidi,[a] Martin A. Montecino,[c] Jane B. Lian,[a] André J. van Wijnen,[d] Janet L. Stein,[a] Gary S. Stein[a]

Department of Biochemistry and University of Vermont Cancer Center, University of Vermont College of Medicine, Burlington, Vermont, USA[a]; Department of Cell and Developmental Biology and Program in Bioinformatics and Integrative Biology, University of Massachusetts Medical School, Worcester, Massachusetts, USA[b]; Center for Biomedical Research and FONDAP Center for Genome Regulation, Universidad Andres Bello, Santiago, Chile[c]; Departments of Orthopedic Surgery and Biochemistry and Molecular Biology, Mayo Clinic, Rochester, Minnesota, USA[d]

Stem cell phenotypes are reflected by posttranslational histone modifications, and this chromatin-related memory must be mitotically inherited to maintain cell identity through proliferative expansion. In human embryonic stem cells (hESCs), bivalent genes with both activating (H3K4me3) and repressive (H3K27me3) histone modifications are essential to sustain pluripotency. Yet, the molecular mechanisms by which this epigenetic landscape is transferred to progeny cells remain to be established. By mapping genomic enrichment of H3K4me3/H3K27me3 in pure populations of hESCs in G_2, mitotic, and G_1 phases of the cell cycle, we found striking variations in the levels of H3K4me3 through the G_2-M-G_1 transition. Analysis of a representative set of bivalent genes revealed that chromatin modifiers involved in H3K4 methylation/demethylation are recruited to bivalent gene promoters in a cell cycle-dependent fashion. Interestingly, bivalent genes enriched with H3K4me3 exclusively during mitosis undergo the strongest upregulation after induction of differentiation. Furthermore, the histone modification signature of genes that remain bivalent in differentiated cells resolves into a cell cycle-independent pattern after lineage commitment. These results establish a new dimension of chromatin regulation important in the maintenance of pluripotency.

Human embryonic stem cells (hESCs) are an increasingly powerful tool for regenerative medicine. They recapitulate, *in vitro*, the molecular phenomena that take place during the first stages of embryonic development. Like their *in vivo* counterparts, ESCs proliferate rapidly and are able to form the three embryonic germ layers (1). This highly self-renewing and pluripotent state is sustained by a unique epigenetic landscape, consisting of transcription factors, chromatin remodeling complexes, and histone modifications that provide the transcriptional plasticity required for rapid response to differentiation cues (2).

Histone H3 lysine 4 and 27 trimethylations (H3K4me3 and H3K27me3, respectively) are key histone modifications that are involved in transcriptional regulation (3, 4). H3K4me3 near transcriptional start sites (TSSs) marks regions of active transcription or transcriptional readiness (5). H3K27me3 modification, in contrast, is a well-established negative regulator of gene expression that repels transcriptional activators and attracts chromatin repressors that promote chromatin compaction (6). Genomic regions that host both histone marks, so-called bivalent domains, were first observed in ESCs, primarily near promoters of genes with developmental functions (7–9). Significant effort has gone into understanding the biological role of bivalency; the consensus is that, in ESCs, it represses transcription but poises genes for rapid expression during lineage commitment (10). Although this proposition is not yet supported with direct evidence, it has become clear that bivalent domains are essential for maintaining ESC pluripotency and self-renewing capacity (10). Despite the extensive availability of genome-wide maps of these histone marks in pluripotent and committed cells, it is not understood how they contribute to faithful reestablishment of transcriptional status after cell division. Compelling questions remain, including the detailed localization of H3K4me3 and H3K27me3 during mitosis, whether these histone marks are gained/lost exclusively during mitosis, and perhaps more importantly, whether they constitute bivalent domains that are retained after cells exit mitosis.

Here, we show that dynamic cell cycle control of H3K4 methylation/demethylation of bivalent genes represents a new dimension to chromatin regulation that advances understanding of how the pluripotent histone modification landscape contributes to maintenance of hESC identity. We developed a new method for isolating pure populations of hESCs at the G_2, mitosis (M), and G_1 phases of the cell cycle and used these phase-specific populations to map the genome-wide distribution of bivalent domains (H3K4me3/H3K27me3) throughout the pluripotent cell cycle. Consistent with a pivotal developmental function, we demonstrate that bivalent genes enriched with H3K4me3 during mitosis are maximally upregulated following induction of hESC differentiation, and subsequently, H3K4me3 on these genes becomes cell

Received 16 September 2015 **Returned for modification** 20 October 2015
Accepted 30 November 2015

Accepted manuscript posted online 7 December 2015

Citation Grandy RA, Whitfield TW, Wu H, Fitzgerald MP, VanOudenhove JJ, Zaidi SK, Montecino MA, Lian JB, van Wijnen AJ, Stein JL, Stein GS. 2016. Genome-wide studies reveal that H3K4me3 modification in bivalent genes is dynamically regulated during the pluripotent cell cycle and stabilized upon differentiation. Mol Cell Biol 36:615–627. doi:10.1128/MCB.00877-15.

Address correspondence to Gary S. Stein, gary.stein@uvm.edu.

Supplemental material for this article may be found at http://dx.doi.org/10.1128/MCB.00877-15.

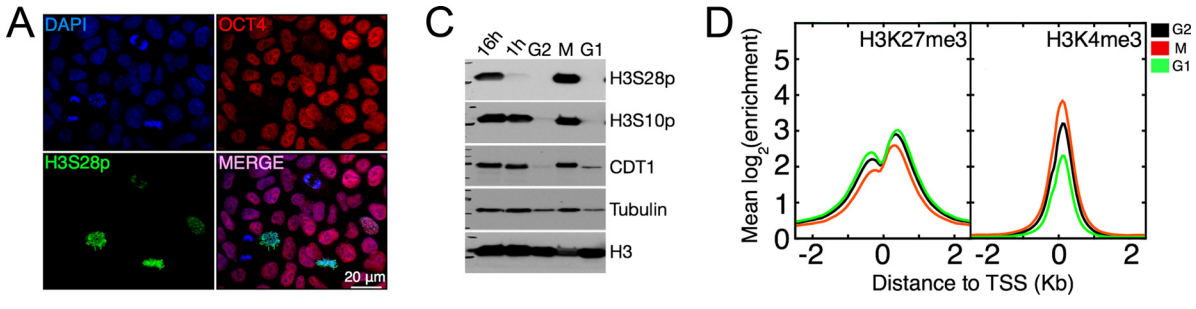

E

Gene Ontology Term	% Genes	p-value
Multicellular Organismal Development	27.3	3.7E-69
System Development	23.4	3.1E-65
Developmental Process	28.6	1.7E-64
Anatomical Structure Development	24.4	9.3E-62
Multicellular Organismal Process	34.0	2.6E-52
Organ Development	18.0	1.1E-51
Cell Differentiation	16.3	1.9E-41
Anatomical Structure Morphogenesis	13.1	3.2E-41
Nervous System Development	12.1	3.8E-39
Cellular Developmental Process	16.5	3.8E-39

FIG 1 Genome-wide mapping of H3K4me3 and H3K27me3 across the cell cycle reveals a highly dynamic landscape of bivalent genes in hESCs. (A) Immunofluorescence microscopy of unsynchronized hESCs showing DNA (DAPI, blue), OCT4 (red), and H3S28p (green). (B) FACS gating parameters used to sort nocodazole-synchronized hESCs into three populations: G_2, mitosis (M), and G_1. (C) Western blot analysis of cell cycle markers H3S28p, H3S10p, and CDT1 in hESCs during nocodazole block (16 h) and 1 h after nocodazole release (1 h) and synchronized cells sorted into G_2, M, and G_1 phases of the cell cycle. Tubulin and total H3 were used as loading controls. (D) Aggregation plots of mean enrichment signal densities for H3K27me3 and H3K4me3. The mean signal densities at G_2, M, and G_1 phases are centered on regions within 2 kb upstream or downstream of TSSs. ChIP-seq enrichment/input in a $\log_2$ scale is displayed. (E) GO term analysis of genes enriched for both H3K27me3 and H3K4me3 during the cell cycle. The percentage of bivalent genes that are represented in each GO term category is also displayed (% Genes).

cycle independent. Finally, we show that chromatin modifiers involved in H3K4 methylation/demethylation are recruited to bivalent gene promoters in a cell cycle-dependent fashion.

MATERIALS AND METHODS

hESC culture and differentiation. The H9 hESC line from WiCell Research Institute (Madison, WI) was maintained on hESC-qualified Matrigel (BD Bioscience; catalog no. 354277) in mTeSR-1 medium (Stemcell Technologies; catalog no. 05850) or essential E8 medium (Life Technologies; catalog no. A1517001), as recommended by the supplier. Cells were expanded every 5 to 6 days, using nonenzymatic passaging according to WiCell Research Institute standard protocols. To generate PAX6 cells, undifferentiated ESCs were incubated in mTeSR-1 medium supplemented with 10 μM retinoic acid (RA) (Sigma-Aldrich; catalog no. R2625-50MG) for 5 days. The treatment started 1 day after plating of the cells, and medium was changed every day. hESC research was approved by the Institutional Embryonic Stem Cell Research Oversight Committee at the University of Vermont.

Cell sorting. Pure populations of cells at the G_2, mitosis, or G_1 phase of the cell cycle were isolated by fluorescence-activated cell sorting (FACS), taking advantage of differences in DNA content to distinguish cells in G_2/M from cells in G_1 and the exclusive presence of histone H3 serine 28 phosphorylation (H3S28p) in mitosis to discriminate cells in G_2 from those in M phase (Fig. 1A and C). As indicated in the figure legends, both nocodazole-synchronized and untreated cells were sorted using the procedure described here. After fixation, cells were permeabilized for 10 min using a mild permeabilization/wash buffer containing saponin (BD Bioscience; catalog no. 51-2091KZ). For ESC isolation, cells were incubated with labeled antibodies to OCT4 (phycoerythrin [PE] conjugated; BD Bioscience; catalog no. 561556) and H3S28p (Alexa Fluor 647 conjugated; BD Bioscience; catalog no. 558609) for 30 min. Labeled antibodies to PAX6, instead of OCT4 (PE conjugated; BD Bioscience; catalog no. 561552) were used to stain PAX6 cells. After staining, cells were washed with permeabilization/wash buffer, resuspended in 2% fetal bovine serum (FBS) in phosphate-buffered saline (PBS), and counterstained with 1 μg/ml 4′,6-diamidino-2-phenylindole (DAPI) (Life Technologies; catalog no. D1306) for 30 min. FACS was performed on a BD FACSAria II cell sorter using linear forward scatter (FSC) and side scatter (SSC) scaling, followed by height- and area-based doublet discrimination. Compensation was calculated using FACS Diva autocompensation algorithms and supplemented by manual compensation to correct for autofluorescence. Cells with subnormal DNA content were filtered out during the gating, and only samples with a purity of 95% or higher were used in the following experiments.

Synchronization of hESCs. Before every cell sorting experiment, cells were allowed to establish robust colonies. Normally, they were collected 4 to 5 days after plating. To improve the cell yield from sorting, in some experiments we synchronized hESCs at either the G_2/M or G_1 phase of the cell cycle 1 day before the collection, by incubation with nocodazole (Sigma-Aldrich; catalog no. M1404-2MG) (200 ng/ml for 16 h when cells were grown in mTeSR-1). Blocking of hESCs in G_2/M phase was reversible, and cells resumed the cell cycle and progressed into G_1 after nocodazole was withdrawn from the culture medium. For cells growing in E8 medium, 25 ng/ml of nocodazole for 16 h was enough to block most of the cells in G_2/M and allowed progression into G_1 after nocodazole was withdrawn from the medium (data not shown). After synchronization, cells were collected as single cells by treatment with Acutase (MP Biomedicals; catalog no. 1000449) and subsequently fixed with 1% formaldehyde for 10

min followed by 5 min of incubation with 0.125 M glycine (Sigma-Aldrich; catalog no. G8790-100G). Cells were counted and stored at −80°C.

Immunofluorescence microscopy. H9 cells were grown on coverslips previously coated with hESC-qualified Matrigel (BD Bioscience; catalog no. 354277). Normally, 3 days after plating, cells were fixed with 1% formaldehyde in PBS for 10 min and processed for immunofluorescence. For PAX6 cells, the fixation was performed at the end of the differentiation protocol. Subsequently, cells were permeabilized in 0.25% Triton X-100 in PBS and blocked with 0.5% bovine serum albumin (BSA) in PBS. Cells were stained with the following antibodies for 1 h at room temperature: anti-OCT4 (Abcam; catalog no. ab1857 [1:2,000]; Santa Cruz Biotechnology; catalog no. sc8628 [1:1,000]), anti-H3S28p (Millipore; catalog no. 07-145 [1:5,000]), or anti-PAX6 (Santa Cruz Biotechnology; catalog no. sc81649 [1:1,000]). Nuclear DNA was counterstained with DAPI (0.1 μg/ml). Secondary antibodies conjugated with Alexa Fluor 594 or Alexa Fluor 488 (1:1,000; Molecular Probes/Invitrogen) were incubated for 1 h in a humidity chamber and at room temperature. Finally, cells were mounted in Prolong-Gold (Invitrogen).

Immunofluorescence analysis for cells in suspension. After cell sorting experiments, the purity of the sorted samples was evaluated by immunofluorescence analysis. Briefly, a small aliquot of sorted cells was spun down on coverslips by using Cytospin4 (Thermo Shandon). Subsequently, cells were stained using the standard immunofluorescence protocol. Anti-Ki67 antibody was used in these experiments (Santa Cruz Biotechnology; catalog no. sc23900).

Immunoblotting. Whole-cell extracts from cell cycle-specific or unsynchronized cells were used to analyze protein expression by Western blotting. The following antibodies were used: anti-H3 (Abcam; catalog no. ab1791 [1:5,000]), anti-H3S28p (Millipore; catalog no. 07-145 [1:5,000]), anti-H3S10p (Upstate; catalog no. 05-598 [1:5,000]), anti-CDT1 (Abcam; catalog no. ab70829 [1:2,000]), antitubulin (Sigma; catalog no. T9026 [1:30,000]), anti-EZH2 (Cell Signaling; catalog no. AC22 [1:1,000]), anti-MLL-C (antiserum [1:1,000]), anti-KDM1 (Abcam; catalog no. ab17721 [1:1,000]), anti-KDM5A (Abcam; catalog no. ab70892 [1:1,000]), and anti-KDM5B (Abcam; catalog no. ab56759 [1:5,000]).

Chromatin immunoprecipitation-quantitative PCR (ChIP-qPCR) assays. Cells at specific phases of the cell cycle, obtained from 3 to 4 different cell sorting experiments, were pooled and treated as a single sample (or biological replicate). Cells were washed twice with PBS and subjected to extraction of nuclei according to the method in reference 11 with modifications. Isolated nuclei were sonicated using a Misonix S-4000 ultrasonic processor (QSonica) to obtain sheared chromatin ranging from 0.2 to 0.6 kb in size. Five hundred nanograms of sheared chromatin was immunoprecipitated overnight at 4°C. Immunoprecipitated complexes were purified using protein G Dynabeads (Invitrogen), washed three times with low-salt buffer (0.1% SDS, 1% Triton X-100, 2 mM EDTA, 20 mM Tris-HCl, pH 8, 150 mM NaCl), once with high-salt buffer (0.1% SDS, 1% Triton X-100, 2 mM EDTA, 20 mM Tris-HCl, pH 8, 500 mM NaCl), once with Tris-EDTA (TE)–NaCl buffer (1 mM EDTA, 10 mM Tris-HCl, pH 8, 50 mM NaCl), and subsequently eluted (SDS 1%, 0.1 M $NaHCO_3$), reverse cross-linked, and quantified by qPCR using specific primers. The following are antibodies used in this assay: anti-H3K4me3 (Abcam; catalog no. ab1012), anti-histone H3 (Abcam; catalog no. ab1791, lot no. GR151029-1), anti-KDM5A (Abcam; catalog no. ab70892, lot no. GR70517-14/GR70517-24), anti-WDR5 (Abcam; catalog no. ab56919, lot no. GR186228), anti-MLL1-473 (kindly donated by Eli Canaani, Weizmann Institute, Israel), anti-MLL2 (Bethyl Laboratories Inc.; catalog no. A300-113A). Primers included PPP1R1A-F (TCCTTCGGTCAGTCTCAAAG), PPP1R1A-R (GACGAACGCTCAGTTTGC), TBX1-F (ATAGGGCGCTGTAAGCAAC), TBX1-R (AAAGGGAAGCACTGAGGAG), TLX2-F (TAGCGGGACTCACCTTCC), TLX2-R (GGAGACGGGGTCAGAGTC), TBC1D20-F (GTAATTACATCGGCGGTACG), TBC1D20-R (GGTATCAGCTCTCCCGAAC), COL1A1-F (TCATCATCTCCCTTCCATTC), COL1A1-R (TACTCTATATCGCGCCTTGC), FOXJ1-F (AGCTGGGGAGGATCTTTTAG), FOXJ1-R (ACCTCGAAGAGGAAAGGAAG), PAX6-F (CTCCAGCAAAACACTTCCTC), PAX6-R (CGGAGTGATTAGTGGGTTTG), CDC25A-prox-F (TGCTCTTCGCCTGCAGCCC), CDC25A-prox-R (CTCTCCGAGGCCGACACCGA), CDC25A-dist-F (ACAGTGGGACCACAGACCATGTG), CDC25A-dist-R (AGCCATGCTGGACAGGTGGA), HOXA4-F (TCTAGGCTAACAGGCGAAAG), and HOXA4-R (GATCTGCGGTTGAGAAAATG).

Chromatin immunoprecipitation sequencing (ChIP-seq) library preparation. Cells at specific phases of the cell cycle, obtained from 3 to 4 different cell sorting runs, were pooled and treated as a single sample (or biological replicate). Two biological replicates were analyzed for each cell cycle phase and for each cellular condition (ESCs and PAX6 cells). Cells were washed twice with PBS and subjected to extraction of nuclei according to the method in reference 11 with modifications. Isolated nuclei were sonicated using a Misonix S-4000 ultrasonic processor (QSonica) to obtain sheared chromatin ranging from 0.2 to 0.6 kb in size (see Fig. S2A in the supplemental material). Sheared chromatin (4 μg) was immunoprecipitated with either anti-H3K4me3 (Abcam; catalog no. ab1012) or anti-H3K27me3 (Millipore; catalog no. 07-449). Immunoprecipitated complexes were purified using protein G Dynabeads (Invitrogen), eluted, reverse cross-linked, quantified, and subjected to library preparation. Immunoprecipitated DNA or input DNA for each cell cycle phase, cellular condition (ESC versus PAX6 cells), and biological replicate was end repaired using the End-It DNA end repair kit (Epicentre), extended using a Klenow fragment (3′-5′ exo) (Epicentre), and ligated to sequencing adaptor oligonucleotides (Illumina), according to the manufacturers' recommendations. Each library was then subjected to 15 cycles of PCR amplification using PFU Ultra II Hotstart master mix (Agilent) and size selected in the range of 300 ± 50 bp. The final libraries were quantified using both Qubit fluorimeter (Life Technologies) and Bioanalyzer (Agilent Technologies) systems and then submitted for sequencing.

ChIP-seq analysis. Single-end 36-base sequencing was performed on an Illumina Genome Analyzer II. Base calls and sequence reads were generated using Illumina CASAVA software (version 1.6; Illumina). Reads were mapped to the human genome (GRCh37, hg19) using bowtie (version 0.12.8) (12) with up to two mismatches allowed. For each cellular condition (i.e., defined by cell cycle phase and differentiation state), genome-wide enrichment profiles were generated from pooled ChIP-seq replicates versus input for H3K27me3 and H3K4me3, respectively, using SPP (13). The resulting enrichment profiles are conservative statistical estimates of $\log_2$ fold enrichment across the genome, corresponding to a 99% confidence interval, $\alpha = 0.01$. The UCSC known gene annotations (14) for canonical transcripts were used to analyze enrichments around transcriptional start sites (TSSs). In order to restrict our analysis to genes enriched for both H3K27me3 and H3K4me3, so-called bivalent genes, we required that for both histone modifications during any pair of cell cycle phases, $\min[\log_2(e_1^j), \log_2(e_2^j), \cdots, \log_2(e_i^j), \cdots, \log_2(e_N^j)] > 1$, where e_i^j is the enrichment at the ith position around the TSS for gene j and N is chosen such that the window within size is 500 bp. That is, bivalent genes were defined to show a 2-fold or greater enrichment everywhere in at least one 500-bp window of the spanned TSS neighborhood (within 2 kb upstream or downstream of the TSS). This restriction resulted in 5,240 bivalent genes. These bivalent genes were examined by direct inspection of the relative H3K4me3 enrichments between different phases of the cell cycle and also using k-means clustering. For the relative H3K4me3 enrichments, the mean ratio of M-phase to G_2-phase or M-phase to G_1-phase enrichments for gene j was calculated as, for example, $[\log_2(M/G_2)] = [\log_2(M)] - [\log_2(G_2)]$, where $[\log_2(M)] = \frac{1}{N'}\sum_{i=-N'/2}^{N'/2} \log_2(e_i^{j,M})$ and N' was chosen to bracket the TSS by 1 kb upstream and downstream. Functional enrichment analysis for the genes grouped by ChIP-seq enrichment patterns used DAVID v. 6.7 (15, 16).

RNA-seq sample preparation. Total RNAs from undifferentiated H9 cells or PAX6 cells were isolated by using TRIzol (Invitrogen). Subsequently, we removed DNA contaminants using a DNA-free RNA extrac-

tion kit (Zymo Research). According to Illumina's recommended protocol, 2 μg of DNA-free total RNA was used to construct each paired-end transcriptome sequencing (RNA-seq) library with the TruSeq RNA sample preparation kit v2 (Illumina). Libraries were subjected to 15 cycles of amplification with pair-end PCR primers (Illumina). Libraries were quantified using a Bioanalyzer system and sequenced on the HiSeq-1000 platform (Illumina) for the read length of 100 bases. To address the influence of culture medium on RNA expression, RNA-seq libraries were built from stocks of ESCs maintained in either mTeSR-1 or essential E8 medium. The RNA-seq libraries for PAX6 cells were generated from original cellular stocks maintained in either mTeSR-1 or E8 medium. No major differences in RNA expression were detected among different stocks. Therefore, libraries of similar cellular condition (control or differentiated) were considered biological replicates.

RNA-seq analysis. Raw sequences from RNA-seq libraries were mapped to genome assembly hg19 using TopHat (version 2.0.8b) (17) with parameters "-b2-sensitive -r 80 -g 10." Mapped reads were analyzed using SeqMonk software (v0.27.0; Babraham Bioinformatics Institute). Expression profiles were calculated using the RNA-seq quantitation pipeline and normalized by globally adjusting count distributions at the 75th percentile. Differential expression was calculated using the intensity difference statistical test included in the software. Differential expression was called on $\log_2$-transformed counts by selecting transcripts that changed with a significance (P) of <0.05 after Benjamini and Hochberg correction using a null model constructed from the 1% of transcripts showing the closest average level of observation to estimate experimental noise. Scatter plots were made using CummeRbund and customized R scripts. Similar results were obtained using Cuffdiff (version 2.1.1).

Inhibition of MLL1/2 proteins in hESCs. H9 cells were grown on hESC-qualified Matrigel (BD Bioscience; catalog no. 354277) in essential E8 medium (Life Technologies; catalog no. A1517001), as recommended by the supplier. After plating (2 days), the cells were preincubated in mTeSR-1 medium supplemented with a cocktail of MLL inhibitors (MLL inh): Mi-2 (Selleckchem; catalog no. S7618) plus MM-102 (Selleckchem; catalog no. S7265), 20 μM each (MLL inh). Control cells were treated with dimethyl sulfoxide (DMSO) only (ATCC; 4×). Eight hours later, cells were exposed to DMSO, nocodazole (200 ng/ml), or nocodazole plus MLL inh, for another 16 h. Subsequently, cells were washed twice with Versene (0.02% EDTA; Lonza; catalog no. 17-711E) and incubated for 10 min in Versene at 37°C, to obtain single cells. Cells were fixed with 1% formaldehyde, counted, and processed for ChIP assays, as described under "Chromatin immunoprecipitation-quantitative PCR (ChIP-qPCR) assays."

For RNA expression assays, the protocol was slightly different. Cells were incubated in mTeSR-1 containing either DMSO or MLL inhibitors for 24 h. Afterward, cells were rinsed twice with Versene and incubated for 10 min in Versene at 37°C, to obtain single cells. Then, cell suspensions were washed twice with fresh essential E6 medium (Life Technologies; catalog no. A1516401) and counted. Cells were seeded at a density of 800,000 cells/well in 6-well plates coated with Matrigel, in essential E6 medium containing retinoic acid (1 μM). Twenty-four hours later, cells were processed for RNA isolation using TRIzol (Invitrogen). Total RNA (1 μg) was used to synthesize cDNA using the SuperScript III reverse transcriptase cDNA synthesis kit (Life Technologies; catalog no. 18064-014). Gene expression was quantified by qPCR using specific primers: PAX6-F (CTTTGCTTGGGAAATCCGAG), PAX6-R (AGCCAGGTTGCGAAGAACTC), HOXA4-F (GCAAGGAGCCCGTGGTGTA), HOXA4-R (GTTGGGCAGTTTGTGGTCTTT), GATA6-F (GCAAAAATACTTCCCCCACA), GATA6-R (CGCCTATGTAGAGCCCATCT), MEIS2-F (AAGGGGGAAGTTTGCAGAGC), MEIS2-R (AATGCATTGGGGGTCCATGT), NANOG-F (CATGAGTGTGGATCCAGCTTG), NANOG-R (CCTGAATAAGCAGATCCATGG), OCT4-F (AGTGAGAGGCAACCTGGAGA), OCT4-R (ACACTCGGACCACATCCTTC), MIXL1-F (GGTACCCCGACATCCACTTG), MIXL1-R (TAATCTCCGGCCTAGCCAAA), SIP1-F (CGCTTGACATCACTGAAGGA), SIP1-R (CTTGCCACACTCTGTGCATT), GAPDH-F (ATGTTCGTCATGGGTGTGAA), and GAPDH-R (TGTGGTCATGAGTCCTTCCA).

Accession number. The Gene Expression Omnibus accession number for the ChIP-seq and RNA-seq data reported in this paper is GSE55502.

RESULTS

Genome-wide mapping of H3K4me3 and H3K27me3 across the cell cycle in hESCs reveals that the bivalent histone modification landscape is highly dynamic. To gain insights into the mechanisms that control the mitotic inheritance of bivalency in pluripotent cells, we globally mapped the genomic locations of the H3K4me3 and H3K27me3 modifications in pure populations of hESCs at the G_2, M, or G_1 phase of the cell cycle, by chromatin immunoprecipitation coupled to high-throughput sequencing (ChIP-seq). To this end, $OCT4^+$ hESCs at G_2, M, or G_1 were isolated by fluorescence-activated cell sorting (FACS), based on both DNA content and H3S28p (histone H3 phosphorylated at serine 28), a mitosis-specific epigenetic mark (18) (Fig. 1A to C). We enriched cultures for mitotic cells by treating them with nocodazole (200 ng/ml, 16 h), a widely used synchronizing agent that has been successfully employed to synchronize ESCs (19–22). Cells in G_1 were purified 1 h after release of the nocodazole block.

The sorted cells exhibited the expected cell cycle-dependent morphological and molecular characteristics (see Fig. S1A in the supplemental material). M-phase cells displayed condensed chromosomes and relatively dispersed OCT4 distribution. G_1 cells were the smallest and exhibited the typical micropunctate pattern for the Ki67 protein (19). G_2 cells were larger than G_1 cells and displayed one or two large Ki67 foci. Biochemical analysis (Fig. 1C) confirmed that H3S28p was exclusive to mitosis (18) and that the licensing factor CDT1 reaches its minimum protein levels in G_2 and its maximum during mitosis (23). Importantly, the protein levels of the pluripotency markers OCT4 and SSEA4 were not affected by the nocodazole treatment (see Fig. S1B). These analyses demonstrate that our strategy yields highly pure populations of hESCs at the G_2, mitosis, or G_1 phase of the cell cycle that are suitable for genome-wide analysis.

Bivalent domains are typically located at gene promoters, and the vast majority of the H3K27me3 modifications observed in ESCs are found in these regions (7, 8). Therefore, we used the more than 15 million uniquely mapped reads generated for each histone mark and cellular condition, to calculate conservative genome-wide ChIP-seq enrichments within regions centered at the canonical TSS (kb ±2) of the UCSC-known genes (Spearman correlations between biological replicates, 0.84 to 0.98 [see Fig. S2E and F in the supplemental material]). We found that about one-third (5,340) of the 17,002 genes modified by H3K4me3 were comodified by H3K27me3. Consistent with previous reports, this group was enriched in genes with developmental functions (Fig. 1E) (7–9). Importantly, the majority of these genes (~3,000) have been previously classified as bivalent in hESCs (24) (see Fig. S2C). The additional 2,154 genes classified as bivalent in our study are also enriched in developmental functions and, on average, displayed H3K4me3/H3K27me3 enrichment comparable to that observed in "established" bivalent genes (see Fig. S2B to D). In general, the enrichment profiles of bivalent genes at G_2, M, and G_1 phases of the cell cycle displayed the narrow peak-like distribution typical for H3K4me3 and the broader domain-like configuration associated with H3K27me3 (Fig. 1D) (8, 9).

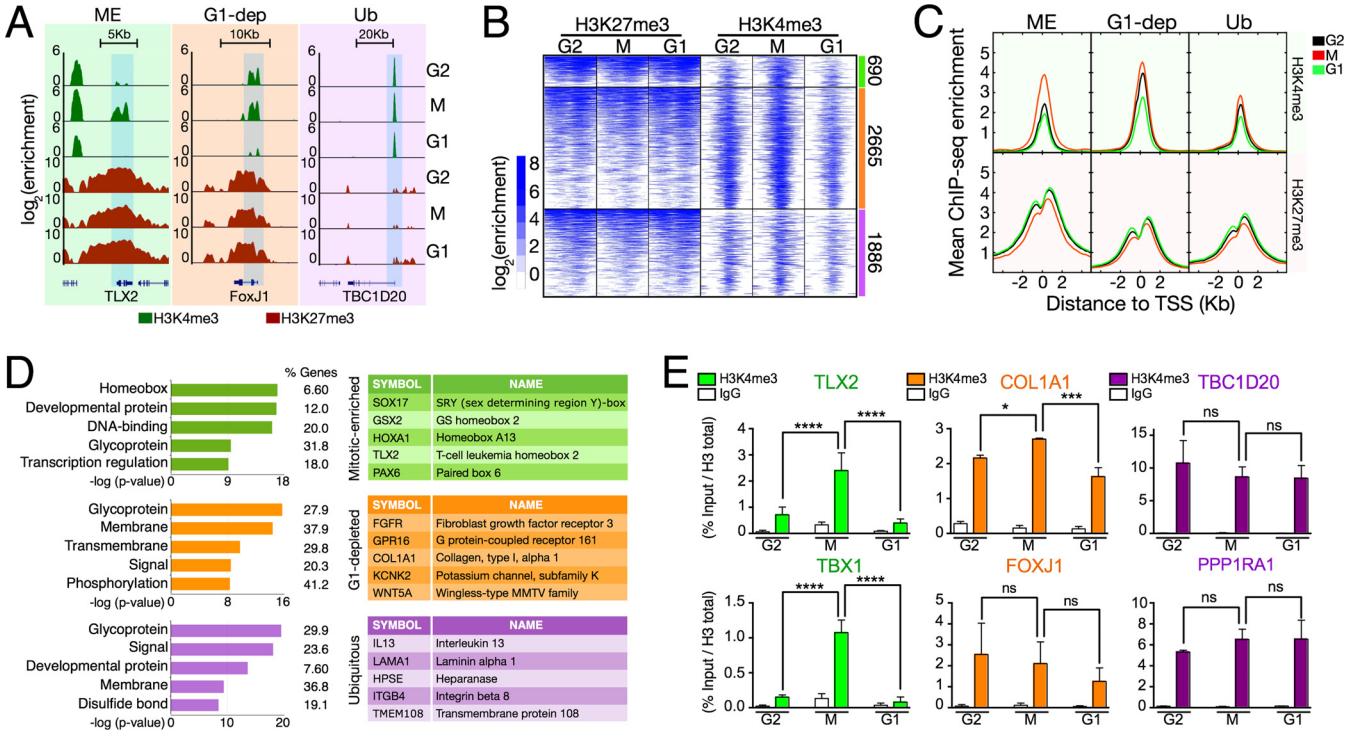

FIG 2 Cell cycle-dependent changes in H3K4me3 define new classes of bivalent genes. (A) ChIP-seq enrichment at select bivalent genes from each of the three cell cycle-dependent bivalency profiles. Shaded areas indicate bivalent domains. ChIP-seq enrichments/input in a $\log_2$ scale are displayed. (B) Heat map of H3K27me3 and H3K4me3 profiles over 4,000-bp regions spanning the TSSs of UCSC canonical genes, grouped according to the divisions illustrated in Fig. S3B in the supplemental material: mitosis enriched (top), G_1 depleted (middle), and ubiquitous (bottom). The total number of genes clustered into each group is displayed on the right. (C) Aggregation plots of H3K4me3 and H3K27me3 ChIP-seq enrichments for bivalent genes clustered according to panel B. (D) GO term analyses of the three groups of bivalent genes clustered by H3K4me3 enrichment profiling. Tables display randomly selected genes from each cluster. (E) ChIP-qPCR analysis of H3K4me3 in hESCs sorted at specific phases of the cell cycle without prior chemical synchronization. Results ($n = 3$) were normalized by total histone H3 levels and expressed as percent input. Ordinary one-way analysis of variance followed by Tukey's test for multiple comparisons was performed. *, $P < 10^{-2}$; ***, $P < 10^{-4}$; ****, $P < 10^{-5}$; ns, not significant.

Interestingly, H3K4me3 levels showed striking variations throughout the cell cycle, reaching maximum enrichment during mitosis and minimum enrichment in G_1 (Fig. 1D): comparing these enrichments, normalized using an MA-norm-like procedure (see below) and averaged over a region within 2 kb upstream or downstream of each TSS, across these three cell cycle phases using Tukey's range test showed that the means differed with a P value of $<7 \times 10^{-5}$. This result correlates well with immunofluorescence analysis showing that there are foci with enhanced H3K4me3 signal during mitosis, compared with cells in interphase (see Fig. S2G in the supplemental material).

In contrast, H3K27me3 levels remained relatively constant across the G_2-M-G_1 transition (Fig. 1D): comparing these enrichments, normalized using an MA-norm-like procedure (see below) and averaged over a region within 2 kb upstream or downstream of each TSS, across these three cell cycle phases using Tukey's range test showed that the means differed relatively little, with a P value of <0.09. Consistently, immunofluorescence assays showed no differences in H3K27me3 levels between mitotic and interphase cells (see Fig. S2H in the supplemental material). Overall, these results indicate that H3K27me3 is stable across the cell cycle, suggesting that this histone mark differs from H3K4me3 not only in its relationship with transcription but also in its regulation throughout the cell cycle.

Cell cycle-dependent changes in H3K4me3 modification define new classes of bivalent genes. Motivated by repeated observations of genes enriched with H3K4me3 during mitosis (mitosis enriched [ME]), genes that exhibited constant levels of H3K4me3 in G_2 and M followed by a pronounced drop during G_1 (G_1 depleted [G_1-dep]), and genes that maintained relatively stable H3K4me3 levels across the cell cycle (ubiquitous [Ub]) (Fig. 2A; see also Fig. S3C in the supplemental material), we classified the bivalent genes into these three categories by defining threshold values for the relevant ratios of mean enrichments (see Materials and Methods and Fig. S3B for details). In this straightforward way, we identified 690 ME genes with levels of H3K4me3 modification at least 2-fold higher during mitosis than in G_2 or G_1, including 28 genes that were manually reassigned based on their histone modification profiles (see Table S1). We found 2,665 G_1-dep genes with similar levels of H3K4me3 in mitosis and G_2 and at least 2-fold-lower levels during G_1 and 1,886 Ub genes with relatively constant levels of H3K4me3 across the cell cycle (Fig. 2B and C; see also Fig. S3C). As an alternative means of classifying cell cycle-dependent H3K4me3 enrichments, k-means clustering ($k = 3$) was applied to the enrichment profiles, after normalizing the ChIP-seq data by either read counts (25) or an MA-norm-like scaling in which linear scaling is used to ensure that the average ChIP-seq enrichment across different cellular conditions is equal over the set of common peaks (26) (see below and Fig. 4D). It is important to note the consistency with which these three cell cycle-dependent signatures were observed, indicating that these his-

tone modification patterns are robust; the same pattern emerges regardless of the data processing method. Throughout the remainder of this paper, the gene classification from Fig. S3B is used.

A more in-depth examination revealed that the ME category includes bivalent genes with the highest levels of H3K27me3 modification (Fig. 2C; see also Fig. S4B in the supplemental material), and gene ontology (GO) analysis revealed that developmentally relevant transcription factor genes are overrepresented in this group (Fig. 2D). Of note, many of these transcription factor genes were marked with H3K4me3 only during mitosis, suggesting stringent cell cycle control of this histone mark (Fig. 2A, D, and E). The Ub and G_1-dep categories displayed comparable average levels of H3K27me3 across the cell cycle (Fig. 2C; see also Fig. S4B), and both include many genes involved in membrane biology and cell signaling; however, the G_1-depleted group uniquely includes genes implicated in phosphorylation processes (Fig. 2D). Overall, these observations suggest a functional separation of genes associated with these three bivalency profiles. Interestingly, we observed genomic regions in which two different cell cycle-dependent bivalency patterns are separated by only a few kilobases (Fig. 2A; see also Fig. S3A). This finding further supports the notion that bivalency is strictly regulated and molecularly compartmentalized during the cell cycle in hESCs.

To validate these results, we carried out ChIP-qPCR analysis from G_2-, M-, and G_1-phase cells isolated from asynchronous hESC cultures (not nocodazole treated) using FACS. Because only limited numbers of mitotic cells are present in asynchronous cultures and H3K27me3 does not vary significantly across the cell cycle, we evaluated H3K4me3 levels for selected genes representative of each of the three bivalency categories. Total levels of histone H3 were assessed to control for possible local variations in nucleosomal density. These experiments corroborated that, in asynchronous cultures, the ME TBX1 and TLX2 genes are modified with H3K4me3 exclusively during mitosis, and H3K4me3 levels in the Ub bivalent TBC1D20 and PPP1RA1 genes do not vary significantly across the cell cycle. Moreover, genes representative of the G_1-dep category, the COL1A1 and FOXJ1 genes, show somewhat reduced levels of H3K4me3 in G_1 (Fig. 2A and E; see also Fig. S3A in the supplemental material).

Taken together, these results reveal unexpected cell cycle-dependent variations in the histone modification landscape that expose previously unknown categories of bivalent genes.

Bivalent genes enriched with H3K4me3 during mitosis experience the strongest upregulation at the onset of hESC differentiation. To understand how the dynamic regulation of H3K4me3 during the pluripotent cell cycle influences transcription of bivalent genes during lineage commitment, we used high-throughput RNA sequencing (RNA-seq). RNA expression levels were analyzed in hESCs before or after induction of retinoic acid (RA) differentiation. As in previous reports (7–9), we found that in undifferentiated hESCs, bivalent genes are either repressed or expressed at very low levels (Fig. 3A). Interestingly, genes in the ME class were the most repressed, whereas those in the G_1-dep group were the least repressed (Fig. 3A). Consistently, genes in the ME class displayed the highest levels of the repressive H3K27me3 mark, and G_1-dep genes showed the highest average levels of H3K4me3 (Fig. 2C). As expected, after inducing differentiation with RA (10 μM, 5 days), we observed downregulation of the pluripotency marker OCT4 and upregulation of the early ectodermal marker PAX6 (Fig. 4A and B) (8). Accordingly, the epigenetic status of the OCT4 promoter changed to a repressed form, with no H3K4me3 and high H3K27me3 (see Fig. S4D in the supplemental material). Likewise, the PAX6 promoter switched from a bivalent, ME state to an active configuration rich in H3K4me3, with very little H3K27me3 (see Fig. S4D). Compared with undifferentiated hESCs, the PAX6-expressing cells (PAX6 cells) displayed significant differential expression of 546 genes ($P < 0.05$) (Fig. 3B). Among these, 138 upregulated genes were bivalent (Fig. 3D). The ME category had the highest proportion of upregulated bivalent genes after RA induction. More importantly, most of these upregulated genes encode transcription factors with developmental functions (Fig. 3D), and they displayed the largest changes in RNA levels in response to RA treatment (Fig. 3C). In contrast, although many genes in the G_1-dep and Ub categories were significantly upregulated, changes in their expression were smaller (Pearson's correlation coefficient $R = 0.661$ for ME genes, $R = 0.876$ for G_1-dep genes, and $R = 0.825$ for Ub genes) (Fig. 3E). These changes are consistent with the H3K4me3 and H3K27me3 ChIP-seq profiles seen in bivalent genes before and after induction of hESC differentiation (see Fig. S4C).

Taken together, these results indicate that bivalent genes which accumulate H3K4me3 modifications during mitosis in pluripotent cells experience more pronounced upregulation at the onset of differentiation. This suggests that these genes are controlled by a distinct mechanism of mitotic chromatin regulation that allows transcriptional activation in response to differentiation cues.

The pluripotent H3K4me3 landscape becomes cell cycle independent upon cell fate commitment. To address whether the cell cycle-dependent, histone modification patterns observed in hESCs are retained in nonpluripotent cells, we generated ChIP-seq libraries for H3K4me3 and H3K27me3 histone modifications from RA-differentiated hESCs (PAX6 cells) synchronized and isolated by FACS at the G_2, M, or G_1 phase of the cell cycle (see Fig. S4A in the supplemental material). Comparison of the H3K4me3/H3K27me3 ChIP-seq profiles obtained in hESCs and PAX6 cells revealed that, although numerous genes lost bivalency after induction of differentiation, many others remained bivalent (Fig. 4C and E; see also Fig. S4C and D). This result was consistent with upregulation of only a fraction of bivalent genes after induction of differentiation (Fig. 3B) and also with reports that the gain or loss of bivalency depends on whether or not genes are activated during a specific lineage-determination process (27, 28).

Importantly, as in ESCs, the average level of H3K27me3 in PAX6 cells remained relatively constant through the G_2-M-G_1 transition, which suggests that the cell cycle-related regulation of H3K27me3 is similar in hESCs before and after the onset of differentiation (Fig. 4C and E; see also Fig. S4B in the supplemental material). In contrast, the H3K4me3 enrichments became cell cycle independent when cells began to differentiate—constant levels of H3K4me3 were observed across the different categories of bivalent genes, during the G_2-M-G_1 transition in PAX6 cells (Fig. 4C to E). Of note, although our initial analysis showed higher levels of the H3K4me3 mark during G_2, these enrichments were abrogated when different types of data normalization were applied (read number versus MA-norm-like scaling normalization) (Fig. 4D).

Together, these results indicate that regulation of H3K4me3 at genes that remain bivalent after the onset of differentiation (PAX6 cells) is cell cycle independent and, furthermore, that the cell cycle-dependent regulation of H3K4me3 modification within bivalent domains is unique to the pluripotent state. This finding is

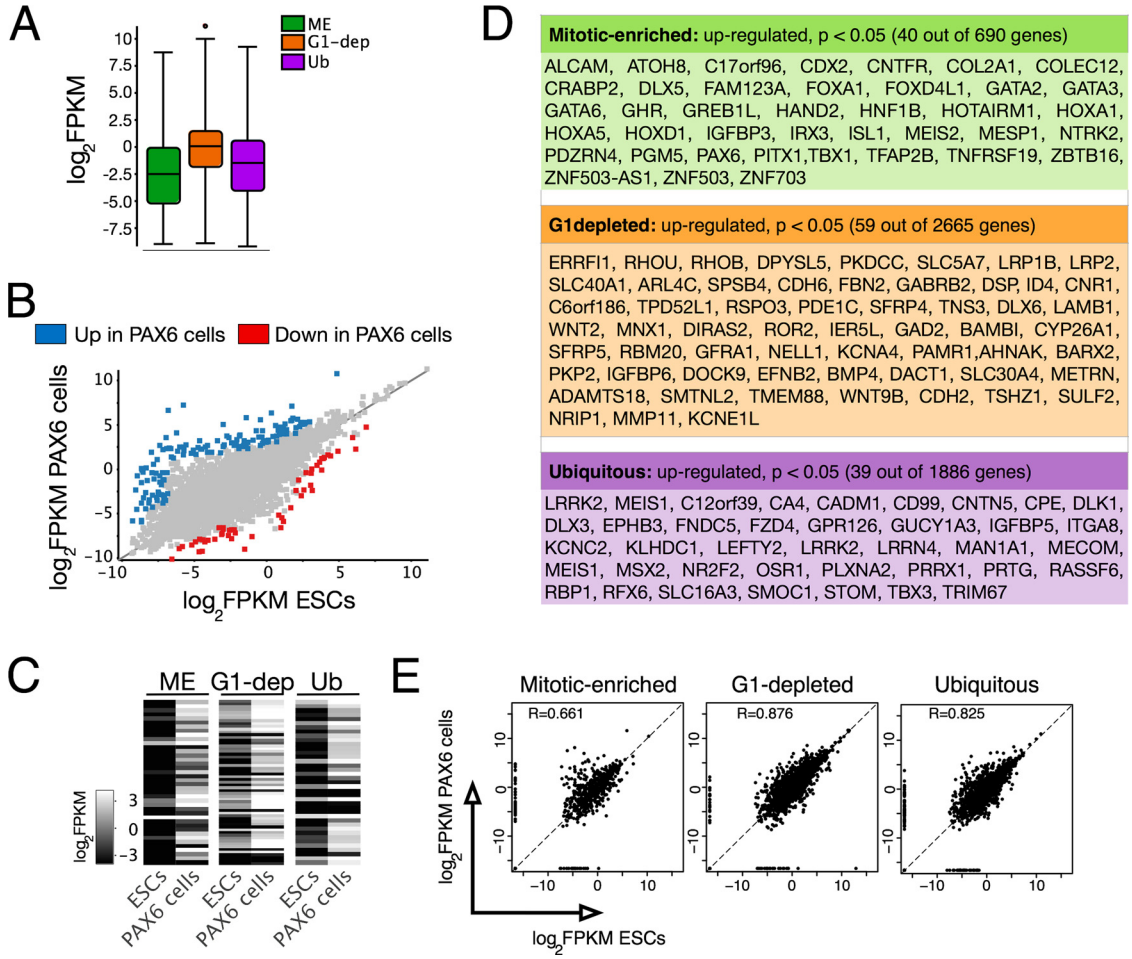

FIG 3 Bivalent genes enriched with H3K4me3 during mitosis experience the strongest upregulation at the onset of hESC differentiation. (A) Box plots for RNA expression (RNA-seq) of bivalent genes in unsynchronized hESCs. The boxes represent the interquartile range (25th to 75th percentiles) for expression of bivalent genes in the indicated categories; the line in the middle of the box represents the median value. (B) Scatter plot demonstrating relative gene expression in hESCs versus PAX6-expressing cells. Genes significantly upregulated or downregulated ($P < 0.05$) in RA-treated, PAX6-expressing cells are highlighted. Genes that remain unchanged are in gray. (C) Heat map of RNA expression levels for bivalent genes upregulated in PAX6 cells. Expression values are presented as fragments per kilobase per million mapped reads (FPKM) on a $\log_2$ scale. (D) List of bivalent genes significantly upregulated in PAX6 cells, displayed for each of the categories of bivalent genes. (E) Scatter plots of RNA expression in hESCs versus PAX6 cells. Expression profiles are displayed for each category of bivalent gene as fragments per kilobase per million mapped reads (FPKM) on a $\log_2$ scale. Pearson correlation coefficients are displayed in the upper left corner of each plot.

consistent with a model in which active accumulation of H3K4me3 during mitosis prepares repressed bivalent genes for activation in response to differentiation cues at the start of the G_1 phase. If those cues do not materialize, H3K4me3 is removed during G_1.

Cell cycle-dependent variation of H3K4me3 correlates with sequential recruitment of KDM5A, MLL1/2, and WDR5. To understand the dynamic regulation of H3K4me3 levels in bivalent genes, we assessed the chromatin occupancy of proteins with H3K4me3 regulatory activity during the pluripotent cell cycle. First, because MLL has H3K4 methyltransferase activity and remains associated with chromatin during mitosis (20), we used ChIP-qPCR to evaluate its interaction with a representative set of bivalent gene promoters during the G_2-M-G_1 transition in unsynchronized hESCs (Fig. 5A). We detected significant MLL binding on promoters of ME genes only during mitosis. Promoters of G_1-dep genes showed modest levels of MLL binding that remained constant during G_2 and mitosis and decreased significantly in G_1. Consistent with expectations, the MLL binding pattern for Ub gene promoters was constant during the G_2-M-G_1 transition. Furthermore, because it was recently shown that MLL2 is the main lysine methyltransferase responsible for H3K4me3 on bivalent genes in mouse ESCs (29, 30), we also assessed the chromatin occupancy of MLL2. Although the binding of MLL2 was modest among the genes evaluated here, the trends were similar to those of MLL cell cycle-dependent binding. Likewise, WDR5, a subunit of the MLL methyltransferase complex that is essential for MLL activity and critical for maintaining ESC self-renewal (3, 31), occupied ME and G_1-dep gene promoters during G_2 and mitosis only, becoming completely dissociated during G_1. Interestingly, a modest but significant enrichment of WDR5 binding was observed during mitosis in ME gene promoters. More importantly, however, no significant cell cycle variation in WDR5 binding to Ub gene promoters was detected.

These results suggest that MLL/WDR5 proteins associate with bivalent gene promoters in a cell cycle-dependent manner that

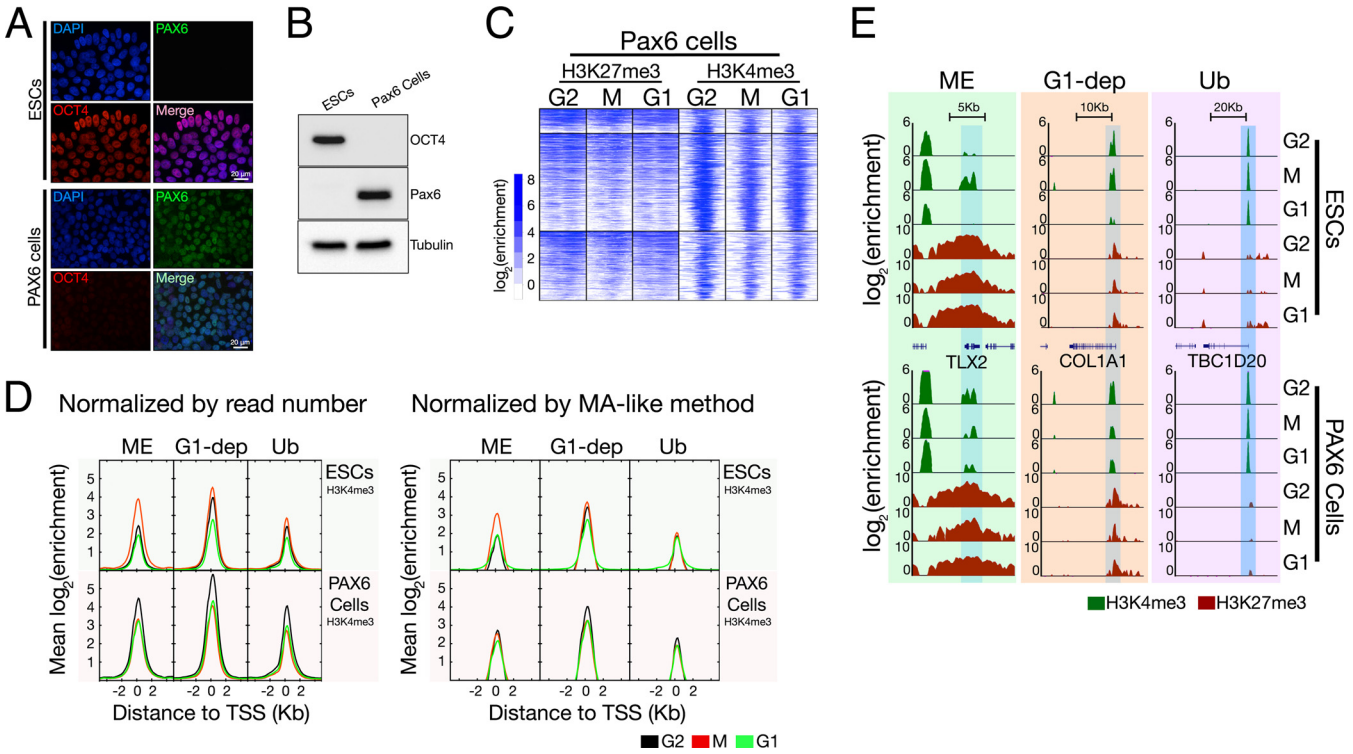

FIG 4 The pluripotent H3K4me3 landscape becomes cell cycle independent upon cell fate commitment. (A) Immunofluorescence microscopy of asynchronous undifferentiated (top) or differentiated (bottom) hESC cultures (retinoic acid, 10 μM, 5 days). Cells were stained for nuclear DNA (DAPI, blue), OCT4 (red), and PAX6 (green). (B) Expression of the pluripotency marker OCT4 and the early differentiation marker PAX6 was analyzed by Western blotting before and after retinoic acid (RA) treatment to induce hESC differentiation. (C) Heat map of H3K27me3 and H3K4me3 profiles observed in PAX6-expressing RA-treated cells. The plot shows ChIP-seq enrichments/input in a $\log_2$ scale for bivalent genes defined in hESCs. (D) Effect of data normalization on the H3K4me3 ChIP-seq enrichments observed during the G_2-M-G_1 transition in undifferentiated and differentiated hESCs. The left panel shows the enrichment profiles after read-number normalization. The right panel shows the enrichment profiles obtained after MA-like data normalization. Note that enrichment of H3K4me3 observed in the G_2 phase of PAX6-expressing cells is not seen when data are analyzed using MA-like normalization. (E) ChIP-seq enrichment at select bivalent genes that exhibit loss of cell cycle-dependent H3K4me3 patterns after induction of differentiation. Shaded areas indicate bivalent domains. As with the undifferentiated hESCs, the ChIP-seq libraries for H3K4me3 and H3K27me3 used in panel C were generated from synchronized $PAX6^+$ cells sorted into G_2, M, and G_1 phases of the cell cycle.

correlates with H3K4me3 enrichment in G_2 and mitosis (Fig. 2). However, they do not explain the reduced H3K4me3 levels observed in G_1 phase. We therefore evaluated KDM5A, a member of the H3K4 di-/tridemethylase family involved in repression of many developmental genes in ESCs (32). Using asynchronous hESC cultures, we found that levels of KDM5A were modestly but significantly enriched in G_1 near ME and G_1-dep gene promoters, which is consistent with the variations in H3K4me3 observed among these genes during the cell cycle (Fig. 5A). Strikingly, the chromatin occupancy of KDM5A on Ub category gene promoters was also significantly increased during G_1 (Fig. 5A). This finding was unexpected because of the constant H3K4me3 levels observed among Ub gene promoters through the cell cycle. However, it is consistent with reports that H3K27me3 facilitates KDM5A recruitment to chromatin (4, 32) and could explain the slight increase in global H3K27me3 levels that we observed in hESCs after mitosis (Fig. 1D). This mechanism would reinforce repression of bivalent genes in pluripotent cells during G_1 phase in the absence of differentiation signals and would be relevant when enzymes with H3K4 methyltransferase activity are not present.

Overall, these results indicate that the methylase/demethylase machinery involved in regulating H3K4me3 levels in hESCs is recruited differentially to bivalent genes in a cell cycle-dependent manner (Fig. 5B). Furthermore, they suggest that similar, related mechanisms may be responsible for the H3K4me3 profiles observed on all bivalent genes.

Disruption of MLL1/2 trimethylase activity abrogates H3K4me3 mitotic enrichment and delays expression of bivalent genes upon induction of cellular differentiation. To further understand the role of H3K4me3 enrichment in bivalent genes during mitosis in pluripotent cells, we assessed the biological consequences of disrupting the activity of the H3K4 trimethylases MLL1/2. Since the genetic ablation of components of the COMPASS complex, including MLL, DPY30, or DWR5 proteins, not only reduces H3K4me3 levels on target genes but also affects the self-renewal capabilities of pluripotent cells (20, 31, 33), we conducted our experiments using less disruptive conditions. We took advantage of two recently developed chemical agents that inhibit MLL1/2 activity, Mi-2 and MM-102. These small nonpeptide molecules decrease H3K4me3 levels on genes by disrupting the interaction between MLL-menin and MLL-WDR5, respectively (34, 35) (Fig. 6A).

Our results show that in hESCs, a 24-h treatment with these inhibitors drastically reduces the levels of H3K4me3 on bivalent genes in mitotic cell-enriched (nocodazole-treated) cultures (Fig. 6B and D), without causing major morphological alterations

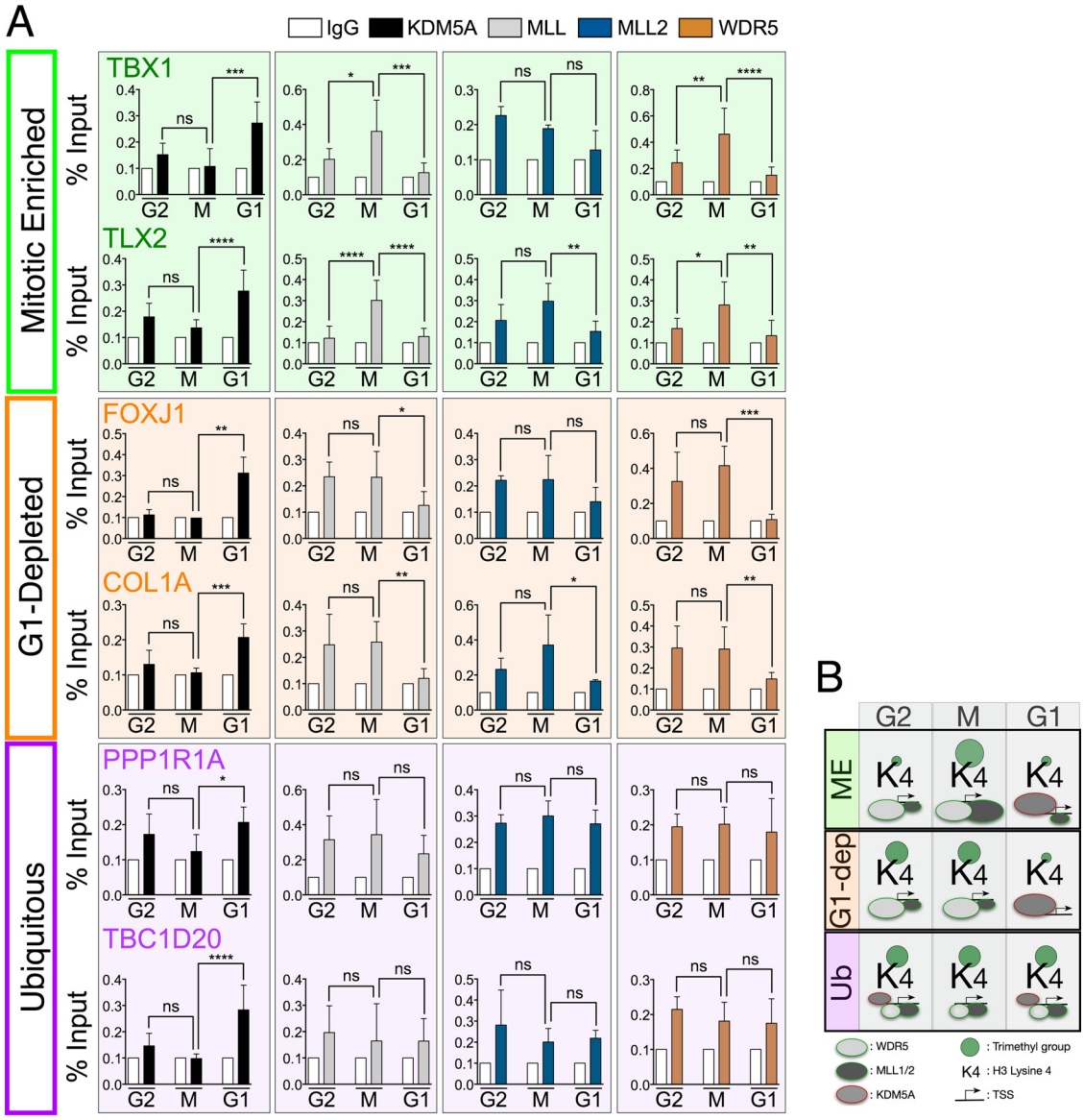

FIG 5 Cell cycle-dependent H3K4me3 variation in ESCs correlates with sequential recruitment of KDM5A, MLL1/2, and WDR5 to bivalent gene promoters. (A) ChIP-qPCR analysis of unsynchronized hESCs sorted at specific phases of the cell cycle, showing the sequential binding of KDM5A and MLL1/2 and the MLL partner WDR5 to bivalent genes. Results are expressed as percent input and are normalized to the IgG control ($n = 3$ for KDM5A and MLL1; $n = 2$ for MLL2 and WDR5). Ordinary one-way analysis of variance followed by Tukey's test for multiple comparisons was performed. *, $P < 10^{-2}$; **, $P < 10^{-3}$; ***, $P < 10^{-4}$; ****, $P < 10^{-5}$; ns, not significant. (B) Summary of the cell cycle-dependent changes observed on histone H3 lysine 4 (K4) in the context of bivalent domains. For simplicity, H3K27me3 is not shown. Sizes of the circles and ovals denote the levels of histone marks or protein enrichments around the TSSs (arrows) of bivalent genes.

(DMSO versus Mi-2/MM-102, 20 μM for 24 h) (see Fig. S5 in the supplemental material). These results further confirmed that H3K4me3 levels are increased during mitosis on certain bivalent genes, such as the PAX6 and HOXA4 genes (from the ME category), and that this phenomenon is dependent on the activity of MLL1/2 complexes (Fig. 6D). As expected, genes from the G_1-dep (COL1A1 gene) and ubiquitous (PPP1RA1 gene) categories did not display H3K4me3 enrichment after synchronization of the cells in mitosis. However, after treatment with MLL1/2 inhibitors, H3K4me3 levels on these genes were reduced (Fig. 6D). Consistent with the distribution of H3K4me3 near the TSSs of genes, the effect of the inhibitors was observed in regions proximal to the TSSs of all the genes analyzed (PAX6, HOXA4, COL1A1, PPP1RA1, and CDC25A genes) but not on a region distal to the TSS (distal CDC25A gene [Fig. 6D]).

Once we established that the acute treatment of human ESCs with a combination of inhibitors successfully inhibited MLL1/2 activity and partially or completely reduced the levels of H3K4me3 on bivalent genes, we assessed the effect on expression of bivalent genes during differentiation. To do this, we incubated cells for 24 h with Mi-2 or MM-102 (20 μM). Subsequently, the MLL1/2 inhibitors were withdrawn; cells were washed with fresh medium, resuspended, and plated as single cells in medium containing RA (1 μM); and then cells were incubated for 24 h (Fig. 6C).

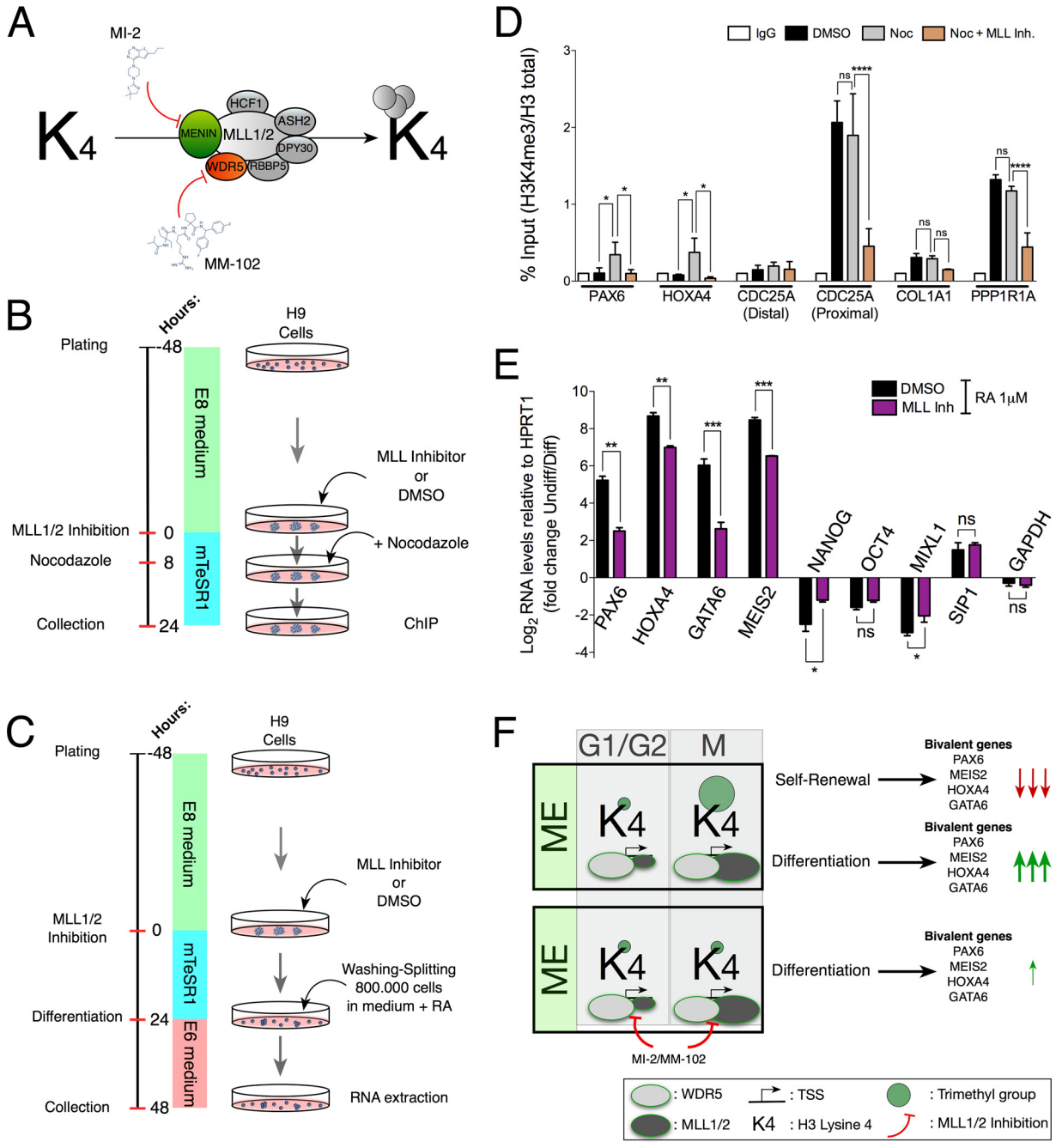

FIG 6 Disruption of MLL1/2 trimethylase activity abrogates H3K4me3 mitotic enrichment and delays expression of bivalent genes upon induction of cellular differentiation. (A) MLL1/2 inhibitors MM-102 and Mi-2 disrupt the interaction of MLL proteins with WDR5 and menin, respectively. (B) Summary of the strategy used to analyze the effect of MLL1/2 inhibitors on H3K4me3 levels in H9 hESCs. Briefly, 2 days after passaging, cells were incubated in mTeSR-1 medium containing Mi-2/MM-102 (20 μM each) for 8 h, followed by 16 h of culture with nocodazole (200 ng/ml) plus Mi-2/MM-102 (20 μM each). Cells were then collected, fixed, and subjected to the ChIP protocol. (C) Strategy used to address the effect of blocking MLL1/2 activity before induction of differentiation in H9 hESCs. Briefly, 2 days after passaging, cells were preincubated in E8 medium containing 20 μM (each) Mi-2 and MM-102 for 24 h. Subsequently, single-cell suspensions were prepared, and 8×10^5 cells were seeded in E6 medium containing 1 μM retinoic acid (RA); 24 h later, total RNA was extracted. (D) ChIP-qPCR analysis of the H3K4me3 levels in hESCs synchronized in mitosis with or without MLL1/2 inhibitors. DMSO, cells treated with DMSO only; Noc, cells blocked in mitosis with nocodazole; Noc + MLL Inh, cells blocked in mitosis with nocodazole in the presence of Mi-2 and MM-102 (20 μM each). Values for percent input are normalized to the IgG control ($n = 2$). One-way analysis of variance followed by Tukey's test for multiple comparisons was performed. *, $P < 10^{-2}$; ****, $P < 10^{-5}$; ns, not significant. (E) Reverse transcription-qPCR analysis of RNA expression levels for bivalent genes after induction of differentiation in unsynchronized H9 ES cells pretreated with MLL inhibitors. Differentiation was induced using E6 medium containing 1 μM RA per 24 h. DMSO, cells pretreated with DMSO only; MLL Inh, cells pretreated with Mi-2 and MM-102 (20 μM each) for 24 h. Unpaired parametric *t* test with Welch's corrections was performed. Two-tailed *P* values were calculated. *, $P < 10^{-2}$; **, $P < 10^{-3}$; ***, $P < 10^{-4}$; ns, not significant. Log_2 RNA levels were normalized against HPRT1 RNA levels and expressed as fold change between undifferentiated and differentiated cells. (F) Summary of the transcriptional outcome of decreasing the mitotic H3K4me3 enrichment in hESCs prior to induction of cellular differentiation. Sizes of the green circles and ovals denote levels of histone marks or protein enrichments around the TSSs (arrows) of bivalent genes. The thickness and number of arrows represent levels of gene expression.

Using qPCR, we found that, in response to RA induction, the expression of ME-category bivalent genes, the PAX6, HOXA4, GATA6, and MEIS2 genes, was reduced or delayed in cells that had been preincubated with MLL1/2 inhibitors, compared to differentiated cells that were not exposed to the MLL1/2 inhibitors (Fig. 6E). Interestingly, inhibition of MLL1/2 prior to the induction of differentiation also delayed the differentiation-dependent repression of genes that are expressed in the pluripotent state (NANOG and MIXL1 genes) (Fig. 6E). Importantly, treatment with MLL1/2 inhibitors did not affect the expression of control genes, the SIP1, glyceraldehyde-3-phosphate dehydrogenase (GAPDH), and HRPT1 genes, indicating that these inhibitors do not alter gene expression globally. This is consistent with the fact that in ESCs, MLL1/2 predominantly catalyze trimethylation of H3K4 on bivalent genes (29, 30).

Together, these results reveal that in hESCs, the inhibition of MLL1/2 activity is sufficient to reduce the levels of H3Kme3 on bivalent genes, which correlates with a delay in the expression of bivalent genes after induction of cellular differentiation (Fig. 6F).

DISCUSSION

The current consensus is that most bivalent genes are largely repressed in pluripotent cells (7, 28, 33) but can rapidly respond to initiators of differentiation by turning on expression in the G_1 phase of the cell cycle (36). Because the G_1 phase in pluripotent hESCs is considerably shorter than that in differentiating cells, it is reasonable to assume that a unique mechanism, active during the M-G_1 transition, is required for cells to mount such a rapid response. In this context, a highly dynamic bivalent landscape may be critical for generating local chromatin conformations that facilitate rapid unfolding of mitotic chromosomes and expedite transcriptional activation in response to differentiation cues during G_1. In this model, genes required for early differentiation are poised for expression only during a very brief window of time, in the context of a transcriptionally unfavorable mitotic environment that prevents unnecessary gene expression. Accordingly, in the absence of differentiation cues, the drastic reduction in H3K4me3 levels observed during G_1 phase would prevent leaky transcription during this phase of the cell cycle when chromatin becomes more accessible. The fact that these histone modification patterns become cell cycle independent after induction of differentiation further supports this scenario and implies that a cell cycle-dependent epigenetic landscape is instrumental in maintaining chromatin architecture plasticity in pluripotent cells but not in committed cells. This is consistent with the finding of Blobel et al. that H3K4me3 remains constant during the G_2-M-G_1 transition in HeLa cells (20). The lengthening of the cell cycle associated with lineage commitment (21, 37) would provide adequate time for cell cycle-independent, expression-regulation mechanisms.

This interpretation is consistent with a recent report from the Vallier lab, documenting that developmental genes not expressed in undifferentiated hESCs become actively transcribed during G_1 phase in response to differentiation cues (36). There is, however, a conflicting recent study reporting that developmental genes are expressed during the G_1 phase of undifferentiated hESCs (38). Importantly, though, this study did not include a selection step to isolate highly pluripotent cells.

Our results reveal the existence of new categories of bivalent domains in ESCs that are associated with genes that have specific cellular functions and expression patterns before and after the onset of differentiation. Importantly, by using a representative set of bivalent genes, we showed that similar cell cycle-dependent histone modification profiles are seen in hESCs purified at G_2, mitosis, and G_1 with or without prior chemical synchronization and that the epigenetic status of these genes correlates with the sequential recruitment of the H3K4 methylase/demethylase enzymatic machinery to chromatin. This is consistent with the fact that the inhibition of MLL1/2 activity decreases the levels of H3K4me3, implying that, after disruption of trimethylase activity, histone demethylases are ready to take over. This mechanism would be important to maintain the dynamic regulation of the H3K4me3 histone mark during the cell cycle.

Of note, hESCs treated to inhibit MLL1/2 activity proliferated at a lower rate than control cells (data not shown); this is consistent with a study reporting that human leukemia cells treated with Mi-2 are arrested in the G_1 phase of the cell cycle (35). This observation suggests that a properly functioning MLL1/2 complex is critical to sustain self-renewal and that the deteriorated self-renewing capability observed in ESCs after knockdown of components of the COMPASS complex may be due more to a lack of H3K4 methylase activity than to the physical absence of these proteins (20, 31, 33). Although inhibition of MLL1/2 trimethylase activity may alter the expression profile of genes necessary for self-renewal, it is also possible that normal patterns of H3K4me3 on bivalent chromatin are required for cells to properly progress through the cell cycle. This is important because it would provide a plausible explanation for the existence of bivalent chromatin domains that do not lose H3K4me3 during the pluripotent G_1 phase (genes in the ubiquitously bivalent category). Whether these bivalent domains are important for cell cycle progression, perhaps by establishing the right conditions for proper DNA replication, is something that should be evaluated in the future.

Importantly, as Pauklin and Vallier showed (36), hESCs respond to differentiation cues during the G_1 phase of the cell cycle. Therefore, it should not be surprising that delaying or arresting G_1-phase progression could have consequences for the timing of cellular differentiation. In this regard, we have shown that decreasing the levels of H3K4me3 on bivalent genes prior to induction of differentiation delayed the expression of critical developmental bivalent genes. This reduced expression seems to be a consequence of impeding the differentiation process, as suggested by the delayed repression of the NANOG gene observed in hESCs induced to differentiate after preinhibition of the MLL1/2 complex.

Overall, our findings strikingly reveal that, at least in pluripotent cells, chromatin structure associated with bivalent genes is not static but dynamically regulated during the cell cycle. The cell cycle-dependent control of epigenetic modification in bivalent domains represents a novel dimension to chromatin regulation that advances understanding of how hESC identity is maintained.

ACKNOWLEDGMENTS

We thank Eli Canaani in the Department of Molecular Cell Biology at the Weizmann Institute of Science, Israel, for donating the anti-MLL473 antibody, Lori Martin-Buley for manuscript editing, Prachi N. Ghule for valuable discussion, the Deep Sequencing Core Facility and Core Flow Cytometry Lab at the University of Massachusetts Medical School, Worcester, MA, the Advanced Genome Technologies Core, and the Flow Cytometry and Cell Sorting Facility at the University of Vermont, Burl-

ington, VT. T.W.W. acknowledges Michael M. Hoffman, Peter Kharchenko, and Anshul Kundaje for helpful discussions.

We declare no conflicts of interest.

FUNDING INFORMATION

HHS | NIH | National Cancer Institute (NCI) provided funding to Gary S. Stein under grant number R01 CA139322. HHS | NIH | National Institute on Aging (NIA) provided funding to Gary S. Stein under grant number RC1 AG035886. Fondo Nacional en Areas Prioritarias (FONDAP; Chile) provided funding to Martin A. Montecino under grant number 15090007.

REFERENCES

1. **Thomson JA, Itskovitz-Eldor J, Shapiro SS, Waknitz MA, Swiergiel JJ, Marshall VS, Jones JM.** 1998. Embryonic stem cell lines derived from human blastocysts. Science **282:**1145–1147. http://dx.doi.org/10.1126/science.282.5391.1145.
2. **Gaspar-Maia A, Alajem A, Meshorer E, Ramalho-Santos M.** 2011. Open chromatin in pluripotency and reprogramming. Nat Rev Mol Cell Biol **12:**36–47. http://dx.doi.org/10.1038/nrm3036.
3. **Shilatifard A.** 2012. The COMPASS family of histone H3K4 methylases: mechanisms of regulation in development and disease pathogenesis. Annu Rev Biochem **81:**65–95. http://dx.doi.org/10.1146/annurev-biochem-051710-134100.
4. **Lanzuolo C, Orlando V.** 2012. Memories from the polycomb group proteins. Annu Rev Genet **46:**561–589. http://dx.doi.org/10.1146/annurev-genet-110711-155603.
5. **Lauberth SM, Nakayama T, Wu X, Ferris AL, Tang Z, Hughes SH, Roeder RG.** 2013. H3K4me3 interactions with TAF3 regulate preinitiation complex assembly and selective gene activation. Cell **152:**1021–1036. http://dx.doi.org/10.1016/j.cell.2013.01.052.
6. **Simon JA, Kingston RE.** 2013. Occupying chromatin: Polycomb mechanisms for getting to genomic targets, stopping transcriptional traffic, and staying put. Mol Cell **49:**808–824. http://dx.doi.org/10.1016/j.molcel.2013.02.013.
7. **Bernstein BE, Mikkelsen TS, Xie X, Kamal M, Huebert DJ, Cuff J, Fry B, Meissner A, Wernig M, Plath K, Jaenisch R, Wagschal A, Feil R, Schreiber SL, Lander ES.** 2006. A bivalent chromatin structure marks key developmental genes in embryonic stem cells. Cell **125:**315–326. http://dx.doi.org/10.1016/j.cell.2006.02.041.
8. **Pan G, Tian S, Nie J, Yang C, Ruotti V, Wei H, Jonsdottir GA, Stewart R, Thomson JA.** 2007. Whole-genome analysis of histone H3 lysine 4 and lysine 27 methylation in human embryonic stem cells. Cell Stem Cell **1:**299–312. http://dx.doi.org/10.1016/j.stem.2007.08.003.
9. **Zhao XD, Han X, Chew JL, Liu J, Chiu KP, Choo A, Orlov YL, Sung WK, Shahab A, Kuznetsov VA, Bourque G, Oh S, Ruan Y, Ng HH, Wei CL.** 2007. Whole-genome mapping of histone H3 Lys4 and 27 trimethylations reveals distinct genomic compartments in human embryonic stem cells. Cell Stem Cell **1:**286–298. http://dx.doi.org/10.1016/j.stem.2007.08.004.
10. **Vastenhouw NL, Schier AF.** 2012. Bivalent histone modifications in early embryogenesis. Curr Opin Cell Biol **24:**374–386. http://dx.doi.org/10.1016/j.ceb.2012.03.009.
11. **Wu H, Whitfield TW, Gordon JA, Dobson JR, Tai PW, van Wijnen AJ, Stein JL, Stein GS, Lian JB.** 2014. Genomic occupancy of Runx2 with global expression profiling identifies a novel dimension to control of osteoblastogenesis. Genome Biol **15:**R52. http://dx.doi.org/10.1186/gb-2014-15-3-r52.
12. **Langmead B, Trapnell C, Pop M, Salzberg SL.** 2009. Ultrafast and memory-efficient alignment of short DNA sequences to the human genome. Genome Biol **10:**R25. http://dx.doi.org/10.1186/gb-2009-10-3-r25.
13. **Kharchenko PV, Tolstorukov MY, Park PJ.** 2008. Design and analysis of ChIP-seq experiments for DNA-binding proteins. Nat Biotechnol **26:**1351–1359. http://dx.doi.org/10.1038/nbt.1508.
14. **Kent WJ, Sugnet CW, Furey TS, Roskin KM, Pringle TH, Zahler AM, Haussler D.** 2002. The human genome browser at UCSC. Genome Res **12:**996–1006. http://dx.doi.org/10.1101/gr.229102.
15. **Huang DW, Sherman BT, Lempicki RA.** 2009. Systematic and integrative analysis of large gene lists using DAVID bioinformatics resources. Nat Protoc **4:**44–57. http://dx.doi.org/10.1038/nprot.2008.211.
16. **Huang DW, Sherman BT, Lempicki RA.** 2009. Bioinformatics enrichment tools: paths toward the comprehensive functional analysis of large gene lists. Nucleic Acids Res **37:**1–13. http://dx.doi.org/10.1093/nar/gkn923.
17. **Trapnell C, Roberts A, Goff L, Pertea G, Kim D, Kelley DR, Pimentel H, Salzberg SL, Rinn JL, Pachter L.** 2012. Differential gene and transcript expression analysis of RNA-seq experiments with TopHat and Cufflinks. Nat Protoc **7:**562–578. http://dx.doi.org/10.1038/nprot.2012.016.
18. **Goto H, Tomono Y, Ajiro K, Kosako H, Fujita M, Sakurai M, Okawa K, Iwamatsu A, Okigaki T, Takahashi T, Inagaki M.** 1999. Identification of a novel phosphorylation site on histone H3 coupled with mitotic chromosome condensation. J Biol Chem **274:**25543–25549. http://dx.doi.org/10.1074/jbc.274.36.25543.
19. **Becker KA, Ghule PN, Therrien JA, Lian JB, Stein JL, van Wijnen AJ, Stein GS.** 2006. Self-renewal of human embryonic stem cells is supported by a shortened G_1 cell cycle phase. J Cell Physiol **209:**883–893. http://dx.doi.org/10.1002/jcp.20776.
20. **Blobel GA, Kadauke S, Wang E, Lau AW, Zuber J, Chou MM, Vakoc CR.** 2009. A reconfigured pattern of MLL occupancy within mitotic chromatin promotes rapid transcriptional reactivation following mitotic exit. Mol Cell **36:**970–983. http://dx.doi.org/10.1016/j.molcel.2009.12.001.
21. **Koledova Z, Kafkova LR, Calabkova L, Krystof V, Dolezel P, Divoky V.** 2010. Cdk2 inhibition prolongs G_1 phase progression in mouse embryonic stem cells. Stem Cells Dev **19:**181–194. http://dx.doi.org/10.1089/scd.2009.0065.
22. **Vihervaara A, Sergelius C, Vasara J, Blom MA, Elsing AN, Roos-Mattjus P, Sistonen L.** 2013. Transcriptional response to stress in the dynamic chromatin environment of cycling and mitotic cells. Proc Natl Acad Sci U S A **110:**E3388–E3397. http://dx.doi.org/10.1073/pnas.1305275110.
23. **Ballabeni A, Melixetian M, Zamponi R, Masiero L, Marinoni F, Helin K.** 2004. Human geminin promotes pre-RC formation and DNA replication by stabilizing CDT1 in mitosis. EMBO J **23:**3122–3132. http://dx.doi.org/10.1038/sj.emboj.7600314.
24. **Li Q, Lian S, Dai Z, Xiang Q, Dai X.** 2013. BGDB: a database of bivalent genes. Database (Oxford) **2013:**bat057. http://dx.doi.org/10.1093/database/bat057.
25. **Bardet AF, He Q, Zeitlinger J, Stark A.** 2011. A computational pipeline for comparative ChIP-seq analyses. Nat Protoc **7:**45–61. http://dx.doi.org/10.1038/nprot.2011.420.
26. **Shao Z, Zhang Y, Yuan GC, Orkin SH, Waxman DJ.** 2012. MAnorm: a robust model for quantitative comparison of ChIP-Seq data sets. Genome Biol **13:**R16. http://dx.doi.org/10.1186/gb-2012-13-3-r16.
27. **Xie R, Everett LJ, Lim HW, Patel NA, Schug J, Kroon E, Kelly OG, Wang A, D'Amour KA, Robins AJ, Won KJ, Kaestner KH, Sander M.** 2013. Dynamic chromatin remodeling mediated by polycomb proteins orchestrates pancreatic differentiation of human embryonic stem cells. Cell Stem Cell **12:**224–237. http://dx.doi.org/10.1016/j.stem.2012.11.023.
28. **Xie W, Schultz MD, Lister R, Hou Z, Rajagopal N, Ray P, Whitaker JW, Tian S, Hawkins RD, Leung D, Yang H, Wang T, Lee AY, Swanson SA, Zhang J, Zhu Y, Kim A, Nery JR, Urich MA, Kuan S, Yen CA, Klugman S, Yu P, Suknuntha K, Propson NE, Chen H, Edsall LE, Wagner U, Li Y, Ye Z, Kulkarni A, Xuan Z, Chung WY, Chi NC, Antosiewicz-Bourget JE, Slukvin I, Stewart R, Zhang MQ, Wang W, Thomson JA, Ecker JR, Ren B.** 2013. Epigenomic analysis of multilineage differentiation of human embryonic stem cells. Cell **153:**1134–1148. http://dx.doi.org/10.1016/j.cell.2013.04.022.
29. **Denissov S, Hofemeister H, Marks H, Kranz A, Ciotta G, Singh S, Anastassiadis K, Stunnenberg HG, Stewart AF.** 2014. Mll2 is required for H3K4 trimethylation on bivalent promoters in embryonic stem cells, whereas Mll1 is redundant. Development **141:**526–537. http://dx.doi.org/10.1242/dev.102681.
30. **Hu D, Garruss AS, Gao X, Morgan MA, Cook M, Smith ER, Shilatifard A.** 2013. The Mll2 branch of the COMPASS family regulates bivalent promoters in mouse embryonic stem cells. Nat Struct Mol Biol **20:**1093–1097. http://dx.doi.org/10.1038/nsmb.2653.
31. **Ang YS, Tsai SY, Lee DF, Monk J, Su J, Ratnakumar K, Ding J, Ge Y, Darr H, Chang B, Wang J, Rendl M, Bernstein E, Schaniel C, Lemischka IR.** 2011. Wdr5 mediates self-renewal and reprogramming via the embryonic stem cell core transcriptional network. Cell **145:**183–197. http://dx.doi.org/10.1016/j.cell.2011.03.003.
32. **Pasini D, Hansen KH, Christensen J, Agger K, Cloos PA, Helin K.** 2008. Coordinated regulation of transcriptional repression by the RBP2 H3K4 demethylase and Polycomb-Repressive Complex 2. Genes Dev **22:**1345–1355. http://dx.doi.org/10.1101/gad.470008.
33. **Jiang H, Shukla A, Wang X, Chen WY, Bernstein BE, Roeder RG.** 2011.

Role for Dpy-30 in ES cell-fate specification by regulation of H3K4 methylation within bivalent domains. Cell **144:**513–525. http://dx.doi.org/10.1016/j.cell.2011.01.020.

34. **Karatas H, Townsend EC, Cao F, Chen Y, Bernard D, Liu L, Lei M, Dou Y, Wang S.** 2013. High-affinity, small-molecule peptidomimetic inhibitors of MLL1/WDR5 protein-protein interaction. J Am Chem Soc **135:**669–682. http://dx.doi.org/10.1021/ja306028q.
35. **Shi A, Murai MJ, He S, Lund G, Hartley T, Purohit T, Reddy G, Chruszcz M, Grembecka J, Cierpicki T.** 2012. Structural insights into inhibition of the bivalent menin-MLL interaction by small molecules in leukemia. Blood **120:**4461–4469. http://dx.doi.org/10.1182/blood-2012-05-429274.
36. **Pauklin S, Vallier L.** 2013. The cell-cycle state of stem cells determines cell fate propensity. Cell **155:**135–147. http://dx.doi.org/10.1016/j.cell.2013.08.031.
37. **Becker KA, Stein JL, Lian JB, van Wijnen AJ, Stein GS.** 2010. Human embryonic stem cells are pre-mitotically committed to self-renewal and acquire a lengthened G_1 phase upon lineage programming. J Cell Physiol **222:**103–110. http://dx.doi.org/10.1002/jcp.21925.
38. **Singh AM, Chappell J, Trost R, Lin L, Wang T, Tang J, Matlock BK, Weller KP, Wu H, Zhao S, Jin P, Dalton S.** 2013. Cell-cycle control of developmentally regulated transcription factors accounts for heterogeneity in human pluripotent cells. Stem Cell Rep **1:**532–544. http://dx.doi.org/10.1016/j.stemcr.2013.10.009.